

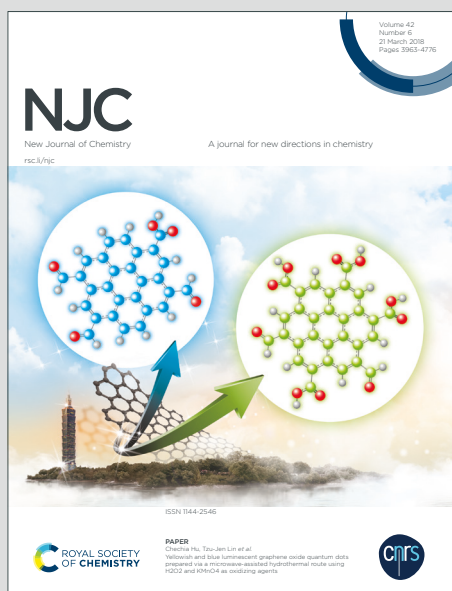
NJC

New Journal of Chemistry

A journal for new directions in chemistry

Accepted Manuscript

This article can be cited before page numbers have been issued, to do this please use: D. Malpicci, D. Maver, D. Maggioni, P. Mercandelli, L. Carlucci, E. Cariati, P. R. Mussini and M. Panigati, *New J. Chem.*, 2023, DOI: 10.1039/D3NJ02823B.



This is an Accepted Manuscript, which has been through the Royal Society of Chemistry peer review process and has been accepted for publication.

Accepted Manuscripts are published online shortly after acceptance, before technical editing, formatting and proof reading. Using this free service, authors can make their results available to the community, in citable form, before we publish the edited article. We will replace this Accepted Manuscript with the edited and formatted Advance Article as soon as it is available.

You can find more information about Accepted Manuscripts in the [Information for Authors](#).

Please note that technical editing may introduce minor changes to the text and/or graphics, which may alter content. The journal's standard [Terms & Conditions](#) and the [Ethical guidelines](#) still apply. In no event shall the Royal Society of Chemistry be held responsible for any errors or omissions in this Accepted Manuscript or any consequences arising from the use of any information it contains.

ARTICLE

Received 00th January
20xx,Accepted 00th January
20xx

DOI: 10.1039/x0xx00000x

2-pyridine cyclic triimidazole as chelating and bridging ligand in mono- and hexanuclear Re(I) complexes with emissive properties in solution and in the solid stateDaniele Malpicci,^a Daniele Maver,^a Daniela Maggioni,^{a,b} Pierluigi Mercandelli,^a Lucia Carlucci,^{a,b} Elena Cariati,^{a,b} Patrizia Mussini,^a Monica Panigati^{*a,b}

Two luminescent Re(I) complexes, namely the mononuclear *fac*-[ReCl(CO)₃(**TT-Py**)] (**1**) and the hexanuclear [Re(μ-Cl)(CO)₃(μ-**TT-Py**)]₂[Re₂(μ-Cl)₂(CO)₆]₂ (**2**), have been isolated in high yields by one-pot reaction between [ReCl(CO)₃] and different amounts of nitrogen rich 2-pyridine cyclic triimidazole (**TT-Py**), which acts as chelating ligand in both derivatives. The metallo-supramolecular cyclic structure of **2**, which can be described as a metallacycle in which two mononuclear units of **1** act as bridging ligands towards two "Re₂(μ-Cl)₂(CO)₆" fragments, has been confirmed by single crystal X-ray diffraction analysis. Both complexes have been fully characterized in solution by 1D and 2D multinuclear NMR spectroscopy. **1** and **2** exhibit photoluminescence at room temperature in solution, with a broad unstructured emission in the 530–570 nm range. The nature of the excited states involved in the electronic absorption spectrum of **1** has been ascertained by a combined density functional and time-dependent density functional (TD-DFT) study. Both compounds exhibit strong aggregation induced emission enhancement (AIEE), which is more pronounced for **2** leading to a solid state photoluminescence quantum yield equal to 2.5% that is one of the highest value ever reported for Re(I) polynuclear metallacycles so far. The versatility of **TT-Py** to adopt variegated coordination modes, previously observed for Cu(I) and Cu(II) derivatives, is confirmed supporting further use of this ligand to obtain new and peculiar emissive mono-, polynuclear and extended coordination systems.

1. Introduction

Pairing transition metals with different organic chromophores has proven as a successful strategy to obtain materials with diversified and intriguing photophysical and optoelectronic properties, dominated by the presence of low-lying triplet (π, π^*) ligand centered (³LC) and/or metal to ligand charge transfer (³MLCT) transitions. A variety of hybrid metal-organic and organometallic compounds find application in organic light emitting devices, imaging, sensing, solar energy conversion and photocatalysis.¹

In this regard, the search for new exo-donor multidentate ligands appears particularly interesting in view of isolating different luminescent polynuclear metal complexes. Interestingly, some of us have recently reported on the versatility of triimidazol[1,2-*a*:1',2'-*c*:1'',2''-*e*][1,3,5]triazine, **TT**, able to coordinate as mono-, bi- and tri-dentate ligand, affording luminescent metal complexes and coordination polymers.² The functionalization of **TT** with a pyridinic fragment results in an enhancement of the **TT** photoluminescent properties and of its coordination ability. In particular, 3-

(pyridin-2-yl)triimidazo[1,2-*a*:1',2'-*c*:1'',2''-*e*][1,3,5]triazine, **TT-Py** (Chart 1), revealed excitation dependent multicomponent emissive behaviour³ and varied (mono-dentate, chelating-bidentate and μ -bridging chelating) coordination modes towards Cu(II)^{2e} and Cu(I).⁴ In fact, **TT-Py**, due to the presence of two nitrogen atoms, namely that on the pyridine ring (N6' in Chart 1) and the other on the imidazolic unit (N5) at a proper distance is able to act as chelating ligand. Moreover, the additional nitrogen atoms of the triimidazole moiety is available to obtain molecular or extended coordination structures.

Besides, tricarbonyl rhenium(I) complexes containing chelating diimine ligands, of general formula *fac*-[Re(CO)₃(N-N)X]ⁿ⁺ (N[^]N = 1,10-phenanthroline or 2,2'-bipyridine, X = anionic or neutral monodentate ligand, with n = 0 or 1, respectively) have been extensively investigated due to their interesting excited state behaviour.⁵ More than four decades after the first studies reported by Wrighton and Morse on these Re(I) complexes,⁶ there is still a high interest towards their photochemical and photophysical properties related to ³MLCT excited states, which can be modulated by the ligand and the medium.⁷ This tunability, together with chemical stability and synthetic flexibility, makes these Re(I) compounds interesting for numerous applications, (*i.e.* luminescent probes for sensing and biological labelling,⁸ electroluminescent devices,⁹ and photocatalysts or photosensitizers in solar energy conversion processes such as H₂ evolution,¹⁰ photocatalytic and electrocatalytic CO₂ reduction¹¹ and dye sensitized solar cells¹²).

^a Dipartimento di Chimica, Università degli Studi di Milano, Via Golgi 19, 20133 Milano (Italy).

^b Consorzio INSTM, Via G. Giusti 9, 50121 Firenze, Italy.

Electronic Supplementary Information (ESI) available: CCDC [2214632–2214633]. For ESI and crystallographic data in CIF or other electronic format see. See DOI: 10.1039/x0xx00000x

Photochemistry of these carbonyl complexes has also played a key role in the development of molecules capable of controlled CO release for biological applications such as treatment of cardiovascular diseases and bacterial infections.¹³

Moreover, *fac*-Re(CO)₃ represents an interesting and versatile metallic corner in one-step and selective synthesis of metallacycles characterized by high stability and solubility.¹⁴ Most of these metallacycles display interesting photophysical and redox properties leading to their applications in host-guest chemistry, photo-catalysis, biological activity and functional molecular devices.¹⁵

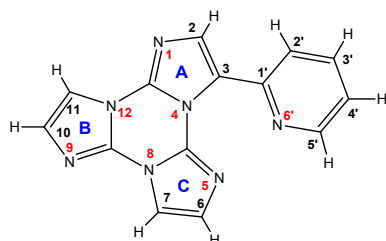


Chart 1. Molecular structure of TT-Py

Starting from these results, we decided to explore the coordination properties of TT-Py with Re(I).

Accordingly, here we report on the synthesis, structural and photophysical characterization of two luminescent complexes obtained by reacting TT-Py and [ReCl(CO)₅] in different stoichiometric ratios. The relationship between structure and emission properties is analyzed also with the support of density functional and time dependent density functional studies (TD-DFT).

2. Results and Discussion

2.1. Synthesis of the rhenium complexes.

Previous results indicated the versatility of TT-Py able to behave towards Cu(II) and Cu(I) both as chelating^{2e} and bridging ligand through the seven-membered chelating ring and one of the three nitrogen atoms of the triimidazole.⁴ We therefore investigated the same versatility towards Re(I) by using different metal:ligand stoichiometric ratios.

The mononuclear [ReCl(CO)₃(TT-Py)] (**1**) and the hexanuclear [{Re(μ-Cl)(CO)₃(μ-TT-Py)}₂{Re₂(μ-Cl)₂(CO)₆}]₂ (**2**) derivatives, shown in Chart 2, were isolated in high yields by treating TT-Py with different amount of [ReCl(CO)₅] in toluene under reflux.

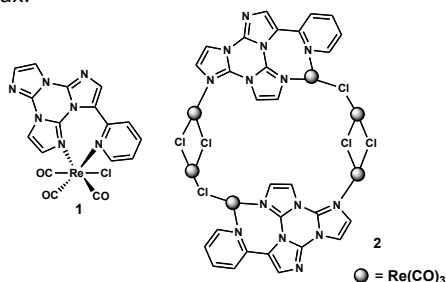
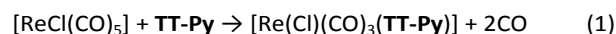


Chart 2. Molecular structures of **1** and **2**

[View Article Online](#)

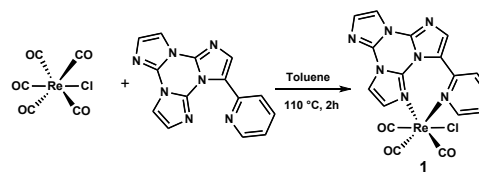
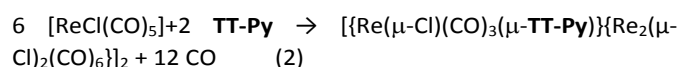
DOI: 10.1039/D3NJ02823B

In particular, **1** was isolated in > 60% yield when TT-Py was reacted with one equivalent of [ReCl(CO)₅] (see eq.1 and Scheme 1).



FTIR monitoring of the reaction after few minutes showed the carbonyl bands of the starting complex together with other three bands in the carbonyl region ($\nu(\text{CO})$ at 2027s, 1925s, 1890s cm^{-1}) (Fig. S1), attributable to a reaction intermediate. Whilst, at the end of reaction, namely after 2 hours, the FTIR spectrum showed three new bands at 2021s, 1909s, 1892s cm^{-1} (Fig. S1), belonging to complex **1**. Both sets of carbonyl frequencies indicate the formation of mononuclear *fac*-rhenium tricarbonyl complexes,¹⁶ where L is a nitrogen ligand and X a halide. Therefore, also considering that at the beginning of reaction TT-Py is in large excess (as a result of the slow dissolution of [ReCl(CO)₅]), the initial set of carbonyl stretching could belong to an intermediate of general formula *fac*-Re(CO)₃(L)₂(X) containing two monodentate terminally coordinated TT-Py ligands. This intermediate very rapidly loses one of the two TT-Py ligands giving complex **1** where, due to the optimized coordination of the chelating TT-Py ligand, an increase of the electron density on the metal is expected. In agreement, the shift at lower wavenumbers of complex **1**, clearly suggests the presence of an electron richer Re atom. Complex **1** is poorly soluble in toluene and, therefore, it gradually precipitated in three hours from the reaction mixture as a white powder.

Besides, by reaction of TT-Py with two equivalents of [ReCl(CO)₅], in toluene solution under reflux, an equimolar mixture of **1** and of the hexanuclear species **2** was obtained in one hour. Conversely, **2** was quantitatively obtained by refluxing in toluene one equivalent of TT-Py with three equivalents of [ReCl(CO)₅], according to eq.2 (see Schemes 2-3). **2** is highly soluble in toluene and, only by adding *n*-hexane, it precipitated as a white-cream solid (isolated yield > 70%).

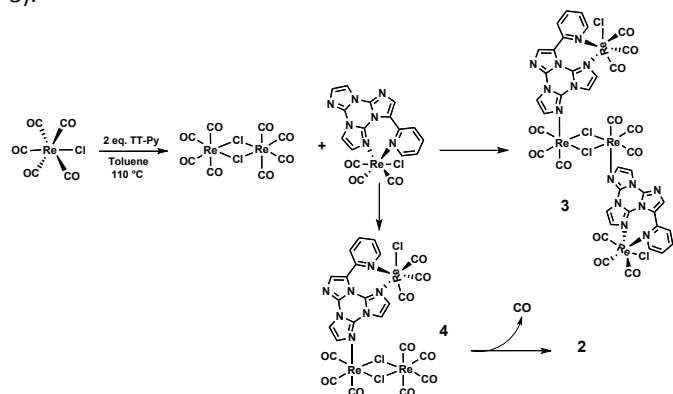


Scheme 1: Synthesis of complex **1**

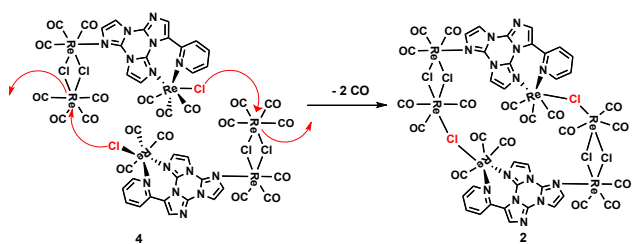
It is interesting to note that a trace amount of **2** was also detected by FTIR in the mother liquor of the reaction of TT-Py with one equivalent of [ReCl(CO)₅] after complete precipitation of **1**. The formation of complex **2** confirmed the possibility of TT-Py to act as bridging ligand, and the possible mechanism of



formation could be described as reported in Scheme 2. In particular, at the beginning of the reaction with two equivalents of metal precursor, the concomitant formation of complex **1** and of the dinuclear complex $[\text{Re}_2(\mu\text{-Cl})_2(\text{CO})_8]$ is observed (FTIR evidence). This dinuclear species, which can be easily obtained by refluxing $[\text{ReCl}(\text{CO})_5]$ in an inert solvent,¹⁷ undergoes decarbonylation reaction faster than $[\text{ReCl}(\text{CO})_5]$, affording the unsaturated $[\text{Re}_2(\mu\text{-Cl})_2(\text{CO})_6]$ fragment (see Scheme 2), which further reacts with complex **1**, affording two possible intermediates (**3** or **4**) which cannot be neither isolated nor spectroscopically revealed. The possible formation of complex **3**, containing two mononuclear complexes terminally coordinated to the $[\text{Re}_2(\mu\text{-Cl})_2(\text{CO})_6]$ fragment (see Scheme 2), whose ratio $\text{Re}/\text{TT-Py}$ is 2/1, is unfavourable due to the progressive precipitation of **1** in toluene. On the contrary, the other possible, more feasible, intermediate **4**, containing only one terminally coordinated mononuclear species and in which the ratio $\text{Re}/\text{TT-Py}$ is 3/1, is not stable and can then dimerize, to give complex **2**, by the fast decarbonylation of the “ $\text{Re}(\text{CO})_4$ ” unit and the following bridging of the chloride ligand. (see Scheme 3).



Scheme 2. Intermediate of reaction with 2 equivalents of $[\text{ReCl}(\text{CO})_5]$



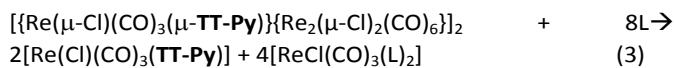
Scheme 3. Dimerization reaction of **4**

From the molecular point of view, **2** can be considered also as a dimeric structure in which two mononuclear **1** units act as

bridging ligands towards two “ $\text{Re}_2(\mu\text{-Cl})_2(\text{CO})_6$ ” fragments. The coordination features of **TT-Py** in **2** resemble that observed in a related Cu(I) coordination polymer⁴ where the ligand acts as a bridging-chelating fragment through the pyridine and imidazole nitrogen atoms.

The nature of both **1** and **2** was established on the basis of spectroscopic data (FTIR and NMR), and was confirmed by single-crystal X-ray diffraction analysis. For complex **2** a $\nu(\text{CO})$ pattern more complex than that of **1** was observed, in agreement with the different symmetries of the many “ $\text{Re}(\text{CO})_3$ ” units present in **2** (see the Experimental Section and Fig. S2).

As many mononuclear rhenium carbonyl complexes, **1** is stable in the solid state, at room temperature and under daylight for different months, if stored under nitrogen. The same stability was observed also in solution, both in non-donor solvents, such as toluene or CH_2Cl_2 , and coordinating solvents such as acetonitrile or DMSO (see Fig. S3-S5 in Supporting Information). On the contrary, complex **2** is less stable in the solid state, even under nitrogen, as shown by the slight change in its FTIR spectrum after one month (See Fig S6). Moreover, complex **2** is completely unstable in donor solvent such as acetonitrile and in weakly coordinating solvents such as THF or MeOH. $^1\text{H-NMR}$ and FTIR spectra (see Supporting Information Fig. S7-S9) clearly indicated that **2** undergoes rapid fragmentation to complex **1** and to $[\text{ReCl}(\text{CO})_3(\text{L})_2]$, with $\text{L} = \text{CH}_3\text{CN}$, THF, MeOH, according to equation 3 (with $t_{1/2}$ values of few minutes in CH_3CN).



2.2. Multinuclear NMR characterization.

^1H NMR spectra of **1** and **TT-Py** in $\text{DMSO-}d_6$ are compared in Fig. 1. Only a partial attribution of the protonic signals could be obtained by the analysis of the ^1H COSY experiment (Fig. S10), since the four CH of imidazole rings B and C (Chart 1) are indistinguishable. After complexation, most of the signals displayed a downfield shift ($\Delta\delta \sim 0.2$ ppm) with the expected largest value for the Hortho of the pyridine ring (H5', 8.66 ppm, $\Delta\delta = 0.73$ ppm). The notable shift displayed by the CH in α position to the pyridine nitrogen atom was mainly due to the charge redistribution after coordination of the pyridine to the metal center (see Tables S1 and S2).



ARTICLE

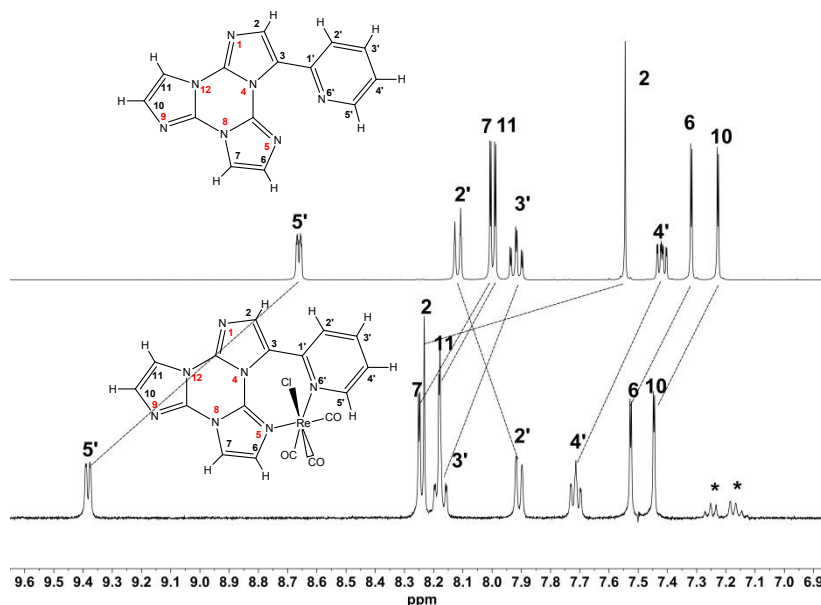


Fig. 1 ¹H-NMR spectra of **TT-Py** (upper trace) and **1** (lower trace) (298 K, DMSO-*d*₆, 7.05 T). Asterisks mark some toluene residue from the synthesis

Despite their distance from coordinating nitrogen atoms N6' and N5, H2' and H2 were highly perturbed upon complexation, showing an upfield ($\Delta\delta = -0.21$ ppm) and a downfield shift ($\Delta\delta = 0.68$ ppm), respectively. These coordination shifts could be ascribed to a major change in their magnetic environment upon re-orientation of the pyridine ring from free to bonded form (see Paragraph 2.3). In fact, differently from its geometry in **1**, in **TT-Py** the H2' points towards the imidazole nitrogen N5 as evidenced from its crystal structures previously reported by some of us.³

To achieve a complete attribution of the protonic signals of **1**, we exploited ¹⁵N NMR spectroscopy carrying out 2D ¹H-¹⁵N heteronuclear long-range correlation (HMBC) experiments (Fig. S11 and S12). As expected, the coordinating imidazole nitrogen N5 showed a substantial change of its chemical shift before and after complexation (-157.3 vs -211.6 ppm, respectively). The attribution of the N5 chemical shift allowed to unequivocally assign H6, and consequently all the other protons of rings B and C. In addition, all the ¹³C signals were attributed through heteronuclear scalar 2D NMR experiments (Fig. S13 and S14). The assignment of all the experimental resonances of **1** was validated by DFT calculations. The whole experimental and calculated ¹H, ¹³C and ¹⁵N NMR chemical shifts are summarized in Table S1.

The ¹H NMR spectrum of **2** was acquired on a sample dissolved in toluene-*d*₈ owing to its insolubility in more polar solvents such as DMSO-*d*₆. This hampered a direct comparison with the signals of **1** in the same solvent. The ¹H spectrum showed the same splitting pattern observed in **1**. The complete attribution of all protonic signals of **2** was accomplished by multinuclear 2D NMR experiments (see Fig. S15-S18). In particular, due to an accidental overlap with the aromatic signals of toluene, it was possible to identify the two imidazole protonic signals only by exploiting the 2D spectroscopy, and in particular the 2D ¹H-¹³C HSQC (see Fig. S16). Nevertheless, as for complex **1**, the ¹⁵N spectroscopy was crucial for the attribution of the ¹H NMR signals, since the typical shift of N9 signal after complexation (from -151.5 to -209.2 ppm) allowed the discrimination of the proton signals of rings B and C, being H10 and H11 immediately recognized and attributed (2D ¹H-¹⁵N HMBC, Fig. S17). To complete the attribution of the quaternary carbon signals, a ¹H-¹³C HMBC experiment was acquired as well (Fig. S18).

The complete attribution of the protonic signals highlighted some notable differences in the ¹H resonance positions with respect to that of the free ligand in the same solvent (see Fig. 2 and S19).

ARTICLE

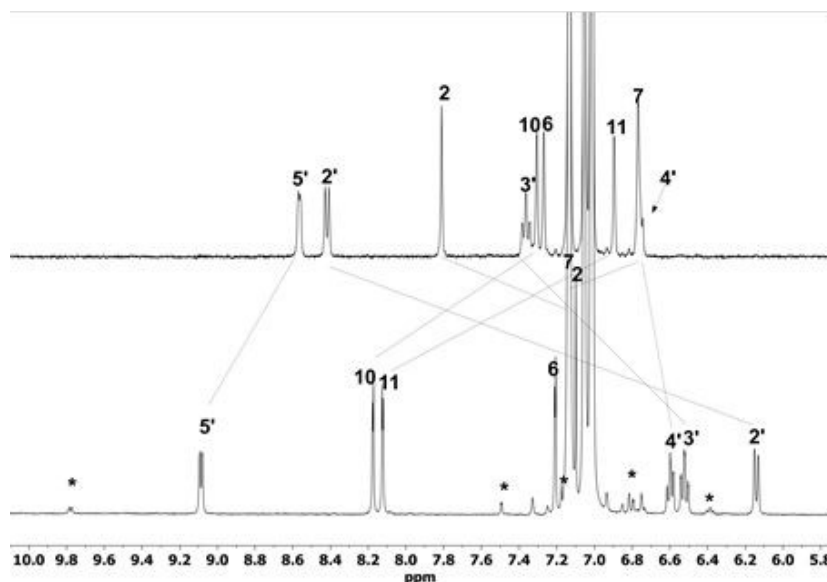


Fig. 2 $^1\text{H-NMR}$ spectra of **TT-Py** (upper trace) and **2** (lower trace) (298 K, toluene- d_6 , 7.05 T). Asterisks mark some signals of small amount of **1**.

Some downfield shifts were easily ascribed to coordination (H5', H10 and H11). On the other hand, H2, H2' and H3' displayed a considerable upfield shift ($\Delta\delta = -0.702, -2.27, -0.835$ ppm, respectively), which were not observed in **1**. A possible origin of these important upfield shifts, assuming a negligible change in the atomic charge distribution upon coordination, could derive from the interaction of toluene with these protons.

The polynuclear nature of **2**, initially suggested by a diffusion NMR experiment (^1H DOSY spectroscopy, Fig. S20) showing a smaller diffusion coefficient for **2** than for **1**, was fully confirmed by single crystal X-ray diffraction analysis (vide infra).

2.3. Structural Characterization.

The structures of **1** and **2** were established by single crystal X-ray diffraction analysis. Fig. 3 and 4 show a picture of the two species, while Table S3 reports some relevant geometrical parameters. In the mononuclear complex **1** the rhenium atom attains an octahedral geometry and bears three terminal carbonyl ligands in a facial arrangement, one terminal chloro ligand and two nitrogen atoms of the chelating **TT-Py** ligand, namely the nitrogen atom of the pyridyl substituent (N7, labelled N6' in the molecular scheme of NMR characterization) and a nitrogen atom of the triimidazotriazine moiety (N3, labelled N5 in the molecular scheme of NMR characterization). The coordination geometry of the rhenium atom resembles that observed in similar *fac*-[ReCl(CO) $_3$ (N $^{\wedge}$ N)] complexes. The conformation adopted by the **TT-Py** ligand is significantly

different from that shown by the free ligand in the solid state.¹⁸ In particular, to allow the ligand to chelate, the pyridyl substituent must rotate around the **TT-Py** bond (as evidenced by the N7–C13–C5–N2 dihedral angle of 46.8°, to be compared to values in the range 144.4–156.1° found in the different polymorphs of the free ligand) and tilt to accommodate the rhenium atom (as evidenced by the N7–C13–C5 bond angle of 123.45°, ten degrees larger than the values in the range 112.46–113.71° found for the free ligand). A similar conformation was adopted by **TT-Py** in previously reported species in which similarly acts as a chelating ligand, namely [Cu $_2$ (**TT-Py**) $_n$]⁴ and [Cu(μ -NO $_3$)(NO $_3$)(**TT-Py**) $_n$]¹⁹ The hexanuclear species **2** (as found in a 2·4(*n*-hexane) crystal) contains two [ReCl(CO) $_3$ (**TT-Py**)] moieties whose geometry is quite similar to that observed in the mononuclear complex **1** (see Table S3). The two [ReCl(CO) $_3$ (**TT-Py**)] moieties bridge two additional [Re $_2$ (μ -Cl) $_2$ (CO) $_6$] fragments through the chloro ligand and a nitrogen atom of the triimidazotriazine moiety (corresponding to N5 in **1**). The geometry of these trans-disubstituted fragments is similar to that observed in similar species, such as [Re $_2$ (μ -Cl) $_2$ (CO) $_6$ L $_2$] (L = MeCN²⁰ and THF²¹). The hexanuclear species **2** shows a non-crystallographically imposed C $_2$ symmetry.



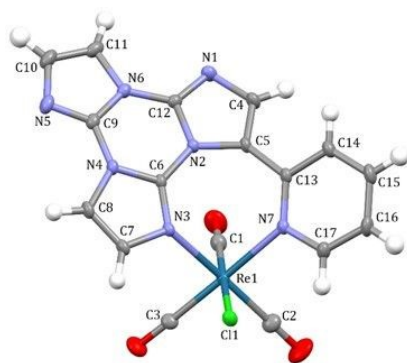


Fig. 3 View of the rhenium complex $[\text{ReCl}(\text{CO})_3(\text{TT-Py})]$ (**1**) as found in its crystal structure, with a partial labelling scheme. Ellipsoids are drawn at 50% probability level.

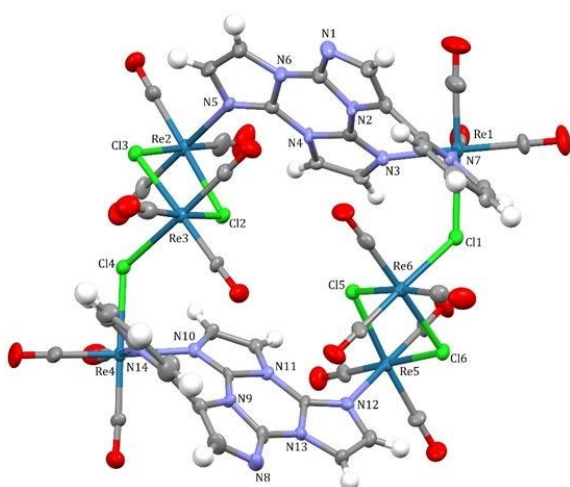


Fig. 4 View of the rhenium complex $[(\text{Re}(\mu\text{-Cl})(\text{CO})_3(\mu\text{-TT-Py}))_2(\text{Re}_2(\mu\text{-Cl})_2(\text{CO})_6)]_2$ (**2**) as found in the crystal structure of its *n*-hexane solvate, with a partial labelling scheme. Ellipsoids are drawn at 50% probability level.

From the crystal structures obtained so far using **TT-Py** as ligand towards Cu(II), Re(I) and Cu(I) it is evident the versatility of this simple molecule able to adopt different coordination modes to give mononuclear, polynuclear and extended 1D structures. In particular, in paddle-wheel dinuclear $[\text{Cu}_2(\text{CH}_3\text{COO})_4(\text{TT-Py})_2]$, **TT-Py** behaved as monodentate through one imidazole nitrogen,⁴ in $[\text{Cu}(\mu\text{-NO}_3)(\text{NO}_3)(\text{TT-Py})]$ it acted as chelating,^{2e} in coordination polymer $[\text{Cu}_2\text{I}_2(\text{TT-Py})]_n$ it was found to bridge through the seven-membered chelating ring and one of the three nitrogen atoms of the triimidazole. Therefore, additional interesting structural motifs are expected by investigating the coordination ability of this ligand with other metals.

2.4. Electrochemical Characterization

Complexes **1** and **2** were investigated by cyclic voltammetry (CV) and selected data are shown in Fig. 5. The study was performed in CH_3CN solution, which in the case of complex **2** enabled to *in*

situ follow its fast solvolysis. into smaller electroactive molecules. DOI: 10.1039/D3NJ02823B

As previously reported²², the **TT-Py** free ligand shows a peculiar first reduction two-peak system at about -2.8 V and -3.1 V vs Fc^+/Fc , which was assigned to a complex electrode process including a series of electron transfer (ET) and chemical steps, starting with radical anion formation, mainly pyridine-centered and kinetically facile. The CV pattern of complex **1** (Fig. 5a) exhibits a quite similar first reduction two-peak system, which points to its first reduction being ligand centered (see also DFT computational part). Such two-peak system exhibits a large shift to less negative potentials respect to the free ligand case (-2.14 V and -2.50 V vs Fc^+/Fc , for C1 and C2 respectively), in agreement with the electron withdrawing effect of the coordinated rhenium center. which makes the ligand much electron poorer.

The first monoelectronic and chemically and electrochemically quasi reversible oxidation peak of complex **1**, at 1.07 V vs Fc^+/Fc , (peak A1 in Fig. 5a) is related to oxidation of the rhenium centre, also consistently with the nature of the HOMO of complex **1** (see below). At the same time, ligand oxidation, observed at ~1.1 V in the case of the free ligand²², because of coordination, must be shifted to more positive potentials, thus possibly corresponding to the second and/or third oxidation peak observed at ~1.6 V/~1.9 V (peaks A2 and A3 in Fig. 5a).²³

Differently from complex **1**, which is stable in the working medium,²⁴ complex **2** undergoes fast solvolysis, affording complex **1** and $[\text{Re}(\text{CO})_3\text{Cl}(\text{CH}_3\text{CN})_2]$. In fact, the CV patterns show the progressive decrease of the oxidation and reduction peaks of **2**, together with the increase of peaks attributed to the decomposition fragments (Figure 5b).

In particular, in the cathodic range, complex **2** shows a similar two-peak system, as observed for complex **1**, with the first reduction peak at less negative potential (-2.01 V, C1' in Figure 5b). This feature can be related to the coordination of the nitrogen of the imidazolic ring with the rhenium atom, making the ligand in complex **2** electron poorer than in complex **1**. Solvolysis starts immediately (C1 peak is already present after one minute; see also NMR evidence, Fig. S9) and is complete after about 20 minutes. Along this period, peak C1' gradually disappears and the first reduction pattern becomes that of complex **1** (C1 and C2 peaks). Moreover, the decomposition process is accompanied by the gradually appearance of another reduction peak at -2.96 V (see C3 in Figure 5b), which is consistent with the $\text{Re}(\text{I})\text{-Re}(\text{0})$ reduction in $[\text{Re}(\text{CO})_3\text{Cl}(\text{CH}_3\text{CN})_2]$.^{11f} It is interesting to note that this reduction is lacking in the CV pattern of complex **1**, due to the higher electron donor capability of **TT-Py**, making rhenium center electron richer and shifting the reduction potential out of the solvent window.

In the anodic part, complex **2** shows two different rhenium oxidation peaks (while A2' and A3' are likely related to the oxidation of the **TT-Py** ligand, see above). The first one (A1 in Figure 5b), lying at the same potential of complex **1**, corresponds to the oxidation of the two rhenium centres



coordinated to **TT-Py** ligand, whose coordination environment is the same as complex **1**. In addition, the peak position supports the lack of electronic communication between the two units forming complex **2**. The second oxidation peak, observed at a more positive potential (at ~ 1.4 V, A1' peak in Fig. 5b), should correspond to the oxidation of the four electron poorer rhenium centers belonging to the "Re(μ -Cl) $_2$ Re" units. During the solvolysis process, A1' gradually disappears while A1 remarkably increases.

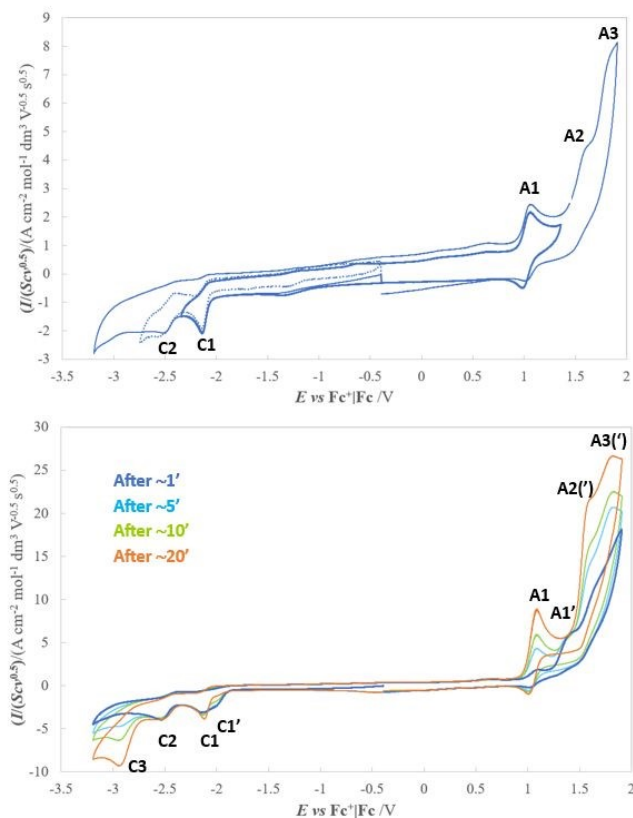


Fig. 5 (a) Cyclic voltammetry of **1** (b) of **2** in CH_3CN , $[\text{NBu}_4]\text{PF}_6$ 0.1 M, using a GC electrode of 3 mm in diameter. Scan rate 0.2 V s^{-1} . Potentials are reported vs. the standard Fc^+/Fc redox couple.

This feature can be justified considering that besides the formation of complex **1**, upon solvolysis, each "Re(μ -Cl) $_2$ Re" moiety affords two $[\text{Re}(\text{CO})_3\text{Cl}(\text{CH}_3\text{CN})_2]$, which should undergo oxidation at the same potential of complex **1**, being coordinated to three CO, one Cl and two N ligands. (although belonging to two acetonitrile molecules instead of a **TT-Py** ligand).²⁵

2.5. Photophysical Characterization

The absorption spectra of the two complexes in diluted CH_2Cl_2 solutions (ca 10^{-5} M) are depicted in Fig. 6a and can be compared with that of the free ligand in the same solvent. **TT-Py** displays two bands at 235 and 290 nm,³ similarly **1** shows two broad bands at 247 and 301 nm (with a shoulder at 314 nm) which, accordingly to electrochemical characterization and to the DFT calculations, correspond to the admixture of different

mono-electronic excitations. In particular, the lower energy band, centred at 301 nm, is due to contributions from metal-to-ligand and halogen-to-ligand charge transfer ($^1\text{MLCT}+^1\text{XLCT}$), with a component of intra-ligand charge transfer (ILCT) from the triimidazotriazine to the pyridyl substituent (see Table 1 and the computational paragraph). Complex **1** displays another broad band, at 247 nm, which is attributable, accordingly to DFT computations, to mainly ligand-centered mono-electronic transitions. However, upon increasing the solvent polarity, from CH_2Cl_2 to MeCN, a clear solvatochromic effect, expected for charge transfer transitions, was not observed (Fig. S21). This feature could be associated to the different nature of the charge transfer electronic transitions contributing in different ways to each of these absorption bands.

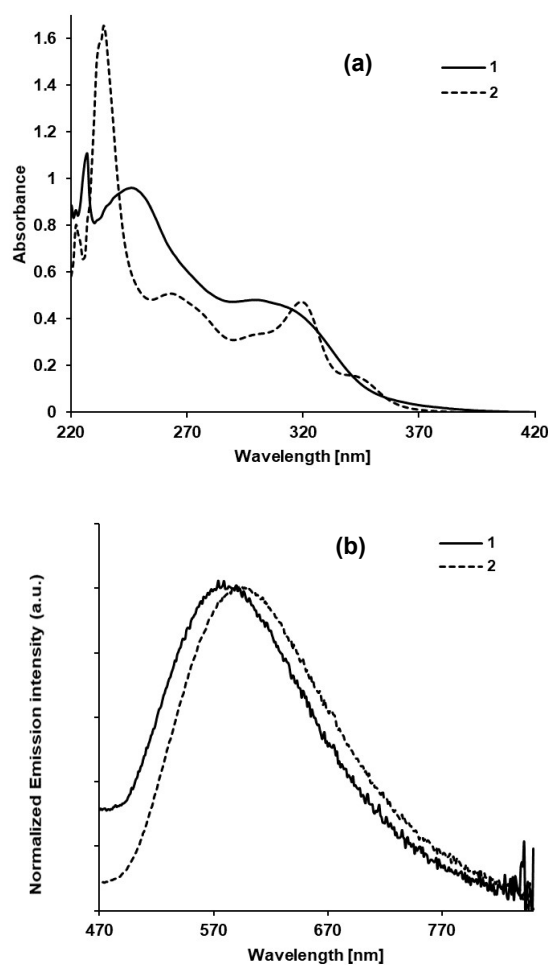


Fig. 6 (a) UV-Vis absorption spectra of **1** (solid lines) and **2** (dotted lines) in CH_2Cl_2 at 298 K; (b) emission spectra in aerated toluene solution at 298 K.

In agreement with the more complex molecular structure of **2**, a larger number of absorption components are observed. Indeed, the spectrum of **2** displays absorptions at 234, 264 and 320 nm, with a shoulder at 346 nm. Unfortunately, a clear attribution of the components was hampered also by the instability of this complex in polar donor solvents, such as MeCN, and by its very low solubility in the most common non-donor polar solvents. However, the electrochemical



characterization clearly indicated that the involvement of the nitrogen N9 of the imidazolic ring, and the chlorine atoms, in the coordination with the "Re(μ -Cl)₂Re" moiety makes easier the reduction on the aromatic ligand, affording a reduction of the HOMO-LUMO gap and a red shift of the corresponding absorption bands. Therefore, we could tentatively ascribe the low energy bands of complex **2** to the same transitions observed for complex **1**.

The photophysical behaviour of both compounds was measured in solution and in the solid state. Upon excitation at 365 nm in toluene (ca 10⁻⁵ M) at 298 K, **1** and **2** display a broad unstructured emission in the visible region (583 and 597 nm, respectively, see Fig. 6b and Table 1). The emission was independent of the excitation wavelengths (see excitation spectra in Fig. S22). Taking into account the computation of the singlet-triplet excitation through TD-DFT calculation (see Computational details and Table S5 in the Supporting Information) and considering the character of the MOs involved (see Fig. S24), the T₁ state responsible for the emission confidently possesses a mixture of metal-to-ligand charge transfer (MLCT) and intraligand (IL) character as already reported for [Cu₂L₂(TT-Py)]_n⁴ and for some Re(I) complexes containing diimine pyridinic ligands.^{5,7} The reduction of the photoluminescence quantum yield (Φ) on going from **1** to **2** (0.4% and 0.01%, respectively), followed by the lengthening of the excited state lifetime (483 and 500 ns, respectively), affords for **2** a k_r value one order of magnitude lower than that of **1** (see Table 1), while the k_{nr} values are identical. This behaviour, which is opposite to what predicted by the energy gap law (where a decrease of the emission energy results into an increase of the non-radiative rate constant k_{nr})²⁶ may suggest that the electronic transitions, responsible for the observed emission in both complexes, are not the same. This difference is in agreement with the more complex molecular and electronic structure of **2**, which, as in the case of the absorption spectrum, hampered an unequivocal attribution of the nature of the excited state responsible of the observed emission.

In the solid state, both derivatives maintain the structureless profile with a concomitant important hypsochromic shift of the emission maxima (532 vs 583 and 563 vs 597 nm, for **1** and **2**, respectively, see Fig. S23). This rigidochromic effect, usually observed for emission from polar excited states, less stabilized by the lack of environment mobility,⁶ suggests a charge transfer character of the emissive state for both complexes. Moreover, the long lifetimes observed for both, in the order of tens microseconds (see Table 1), agree with the phosphorescent character of their radiative deactivation.

Together with the shift, both complexes also exhibit an increase in the photoluminescence quantum yield on moving to the solid state. In particular, for **1**, Φ increases from 0.4 to 12%, (see Table 1), while for **2**, this behaviour is much more pronounced with Φ equal to 2.5%, a value almost 250 times higher than in toluene solution. The emission enhancement of **2** is accompanied by a strong decrease of the radiationless rate constant (k_{nr}) which drops from 1.99×10⁶ to 2.21×10⁴ s⁻¹, going from solution to the solid state, whilst the radiative rate

constant (k_r) remains of the same order of magnitude. For complex **1** the reduction of the k_{nr} is of three order of magnitude on moving from solution to the solid state (2.06×10⁶ vs. 6.15×10³ s⁻¹). These data agree with the hypothesis that the restriction of the vibrational motions is most likely responsible for the enhancement of the emission observed in the solid state, for both complexes, indicating the presence of Aggregation Induced Enhancement Emission (AIEE) effect.²⁷ Indeed, all the alternative mechanisms proposed to explain the aggregation induced emission does not appear at work here, as structural data rule out any close intermolecular interactions. Moreover, looking at the structure of **2**, and considering its very low stability also in poorly coordinated solvents (see above), it is reasonable to suppose that a possible reversible bridge opening and fast interchange between bridging and terminal coordination of the chloride ligands occurs, affording a fast and reversible opening of the circular structure. These features could explain the stronger AIEE effect observed for **2** whose emission, differently from **1**, is almost completely quenched in solution and stronger in the solid state due to the lower mobility imposed by the more rigid environment.

It is important to note that, while AIEE behaviour has already been reported for several Re(I) mononuclear complexes, (with Φ up to 59%),²⁸ and for dinuclear complexes (with Φ up to 56%)^{7f} far less examples of polynuclear compounds, containing more than two rhenium atoms and based on Re(I) molecular rectangles (with Φ around 0.65 %) have appeared in the literature.²⁹ Among these latter, Φ reported for **2** represents a record.

2.6. Computational Study

The electronic structure of complex **1** and its absorption spectrum were computed employing density functional and time-dependent density functional theory. Fig. S24 shows some relevant molecular orbital plots while Tables S4 and S5 report some calculated electronic transition properties.

According to the calculations, in **1** the rhenium d orbitals mainly contribute to the three highest occupied molecular orbitals (HOMOs), lying close together in energy. The three HOMOs show, in addition, significant antibonding interactions with the π orbitals of the halogen atom and bonding contributions from the π^* orbitals of the carbonyl ligands. Lying at lower energy, HOMO-3 and HOMO-4 are ligand π orbitals, mainly located on the pyridyl substituent (HOMO-3) and the triimidazotriazine rings (HOMO-4). The three lowest unoccupied molecular orbitals (LUMOs) are π^* orbitals delocalized all over the organic ligand. In particular, LUMO and LUMO+1 show an important contribution from the pyridyl substituent while LUMO+2 is delocalized over the triimidazotriazine rings only.

The band at lower energy in the absorption spectrum of **1** can be assigned to the superposition of two electronic transitions, S₀→S₄ and S₀→S₅ (computed at 305 and 299 nm, and experimentally observed at 301 and 246 nm, respectively, in CH₂Cl₂, see above), corresponding to the admixture of HOMO→LUMO+1 and HOMO-3→LUMO mono-electronic

excitations. According to the nature of the orbitals involved, and taking into account the difference between the computed atomic charges for the ground and the excited states, both transitions imply a significant metal-to-ligand and halogen-to-ligand charge transfer. The lower-energy transition, however, shows also an important intraligand character (in particular, a net charge transfer from the triimidazotriazine rings to the pyridyl substituent). Two intense electronic transitions, $S_0 \rightarrow S_{19}$ and $S_0 \rightarrow S_{21}$ (computed at 251 and 244 nm, respectively), are

responsible for the peak experimentally observed at ca. 250 nm, see later. They correspond to some complex admixtures of many mono-electronic excitations, mainly HOMO-3 \rightarrow LUMO+2 and HOMO-4 \rightarrow LUMO+1. Both electronic transitions can be described as ligand centered. However, the first one mainly implies a redistribution of the electron density within the TT rings while the second one shows also a sizeable charge transfer from the triimidazotriazine moiety to the pyridyl substituent.

Table 1: Absorption and emission spectral data of **1** and **2** at room temperature.

Complex	λ_{abs} [nm]	$\lambda_{\text{em}}^{\text{[a]}}$ [nm]	$\lambda_{\text{em}}^{\text{[b]}}$ [nm]	Φ % ^[a]	Φ % ^[b]	τ [a] [ns]	τ [b] [μ s]	k_r (s ⁻¹)	k_{nr} (s ⁻¹)
1	247, 301, 314	583	532	0.4	12.0	483	85, 143	8.28×10^3 (1.05×10^3) ^[b]	2.06×10^6 (6.15×10^3) ^[b]
2	234, 264, 320, 346	597	563	0.01	2.5	500	15, 35, 82	2.00×10^2 (5.68×10^2) ^[b]	1.99×10^6 (2.21×10^4) ^[b]

^[a] In aerated toluene solution ($\lambda_{\text{ex}} = 365$ nm). ^[b] In the solid state ($\lambda_{\text{ex}} = 365$ nm).

3. Conclusions

The versatility of the nitrogen-rich derivative of cyclic triimidazole, **TT-Py**, bearing a 2-pyridine substituent on the triimidazole scaffold, was exploited together with the attractive properties of the robust and stable *fac*-Re(CO)₃ core, for the synthesis of the mononuclear complex **1**, and polynuclear **2**. This latter represents one of the few examples of Re(I) hexanuclear derivatives reported in the literature so far.³⁰

1 and **2** could be selectively obtained by varying the **TT-Py**/[ReCl(CO)₃] stoichiometric ratio and were fully characterized in solution by FTIR and multinuclear NMR spectroscopies. This last one was particularly useful for ascertain that the nature of the two complexes in solution was the same as the one observed in the solid state by single crystal X-ray diffraction.

As previously reported for Cu(I) and Cu(II) derivatives with the same ligand, in both **1** and **2** the rotation of the pyridine fragment around **TT-Py** bond allowed the formation of a seven-member ring with the "Re(CO)₃Cl" unit. Moreover, in **2**, as already reported for Cu(I), **TT-Py** acted also as bridging ligand through one nitrogen atom of the triimidazole core affording, through the very simple one-pot synthetic approach, the hexanuclear cyclic structure. In this case, thanks to the bridging coordination ability of chloro ancillary ligand no 1D coordination chain was obtained.

Both complexes displayed interesting photophysical properties in solution and in the solid state where **2** showed a record value of Φ among polynuclear rhenium(I) complexes. These results represent a springboard for the use of other pyridinic substituted TT derivatives as ligands to be exploited for the obtainment of both molecular and, desirably, extended Re(I) tricarbonyl luminescent materials.

4. Experimental

4.1. General procedures and instruments

All the manipulations were carried out in an inert atmosphere (N₂) using dried glassware with the Schlenk technique. The solvents were distilled by standard methods before use. FTIR spectra were acquired on a PerkinElmer Frontier in solution. Elemental analyses were performed on a PerkinElmer CHN2400 instrument. ESI-MS spectra were recorded on a LCQ Fleet ion trap mass spectrometer (Thermo Fisher).

The deuterated solvents (CIL) for NMR spectroscopy were used as received. NMR spectra were acquired on a Bruker Avance DRX-400 equipped with a Bruker 5 mm BBI Z-gradient probe head with a maximum gradient strength of 53.5 G/cm, and operating at 400.13, 100.62, and 40.55 MHz for ¹H, ¹³C and ¹⁵N, respectively. The 90° pulses were calibrated resulting in the following pulse lengths: 8.5 μ s (¹H), 13 μ s (¹³C), and 28 μ s (¹⁵N). NMR samples were prepared by dissolving a few milligrams in 600 μ L of either DMSO-*d*₆ or toluene-*d*₈ to obtain clear solutions in a disposable NMR tube. ¹H NMR spectra were recorded by accumulating 32 transients with a recovery delay of 10 s on a sweep width of 15 ppm. ¹⁵N NMR spectra were referenced to external CH₃NO₂. The experiments were all collected at 300 K using standard 1D and 2D sequences of the Bruker library. The ¹H diffusion spectroscopy (¹H DOSY) was carried out by using the sequence ledbpgp2s incorporating bipolar gradient pulse, incrementing the gradient strength (G) in 16 steps from 5% to 95% by following a sine-shaped function. A diffusion time of 100 ms and a gradient pulse duration of 4 ms were used. **TT-Py** was synthesized as reported in the literature.³

4.2. Synthesis of the Complexes



Synthesis of 1: reaction of TT-Py with one equiv. of [ReCl(CO)₅]. A solution containing TT-Py (20.1 mg, 0.0730 mmol), and an equimolar amount of [ReCl(CO)₅] (27.4 mg, 0.0730 mmol) in 5 mL of freshly distilled toluene was stirred under reflux. The colour of the solution became progressively pale yellow and after a few minutes, complex **1** began to separate as a white precipitate. The solution was stirred for 2 h; then the white precipitate was separated by filtration from the pale yellow solution and it was washed with freshly distilled toluene (3×5mL). The white residue was dried under vacuum yielding 27 mg (0.0465 mmol) of **1** (yield 63%). ¹H NMR (DMSO-*d*₆, 300 K) δ 9.38 (dd, 1H, ³J_{HH} 5.8 Hz, ⁴J_{HH} 1.2 Hz, H5'), 8.25 (d, 1H, ³J_{HH} 2.0 Hz, H7), 8.23 (s, 1H, H2), 8.18 (d, 1H, ³J_{HH} 1.7 Hz, H11), 8.20 (ddd, 1H, ³J_{HH} 7.9 Hz, ³J_{HH} 5.8 Hz, ⁴J_{HH} 1.2 Hz, H3'), 7.91 (dd, 1H, ³J_{HH} 7.9 Hz, ⁴J_{HH} 1.0 Hz, H2'), 7.72 (ddd, 1H, ³J_{HH} 7.65 Hz, ³J_{HH} 5.8 Hz, ⁴J_{HH} 1.0 Hz, H4'), 7.52 (d, 1H, ³J_{HH} 2.0 Hz, H6), 7.45 (d, 1H, ³J_{HH} 1.7 Hz, H10). ¹³C NMR (DMSO-*d*₆, 300 K) δ 196.3 (CO), 195.5 (CO), 189.7 (CO), 155.8 (CH5'), 152.8 (C1'), 140.4 (CH3'), 140.1 (C4a) 139.7 (C12a), 135.3 (C8a), 135.0 (CH2), 131.2 (CH6), 131.2 (CH2'), 129.9 (CH10), 126.9 (C3), 125.0 (CH4'), 114.2 (CH7), 112.9 (CH11). ¹⁵N NMR (DMSO-*d*₆, 300 K) δ -146.8 (N6'), -154.1 (N1), -154.3 (N9), -211.6 (N5), -219.7 (N8), -220.8 (N12), -227.4 (N4). IR (DMSO) ν(CO): 2021 (s), 1909 (s), 1892 (s), cm⁻¹. ESI-MS: *m/z* 603.99 [M-Na]⁺. Elemental anal. calcd for C₁₇H₉ClN₇O₃Re: C 35.11, H 1.55, N 16.87. Found: C 35.19, H 1.56, N 16.85. Crystals of **1** were obtained from slow diffusion of ethyl ether into a nitromethane saturated solution of **1**, at 248 K for a few days.

Reaction of TT-Py with two equiv. of [ReCl(CO)₅]. A solution containing TT-Py (18.4 mg, 0.0668 mmol), and an two equivalents of [ReCl(CO)₅] (48.7 mg, 0.1346 mmol) in 8 mL of freshly distilled toluene was stirred under reflux. The colour of the solution became progressively pale yellow and, after a few minutes, complex **1** began to separate as a white precipitate. The FTIR monitoring of the reaction showed the concomitant formation of complex **2**. The solution was stirred for 2 h; then the white precipitate was separated by filtration from the pale yellow solution, containing complex **2**. The precipitate was washed with freshly distilled toluene (3×5mL), dried under vacuum yielding 10 mg (0.0172mmol) of **1** (yield 12.8%). The solution was evaporated to dryness and dryness under reduced pressure to give a pale yellow solid, which was dissolved in CH₂Cl₂ and precipitated with n-hexane yielding 26 mg (0.0109 mmol) of microcrystalline powder of **2** (yield 48.6%)

Synthesis of 2: reaction of TT-Py with three equiv. of [ReCl(CO)₅]. In order to selectively synthesise complex **2**, TT-Py (20.1 mg, 0.0730 mmol), and [ReCl(CO)₅] (80.6 mg, 0.223 mmol), corresponding to three equivalents, were dissolved in 10 mL of freshly distilled toluene and the solution was stirred under reflux. The colour of the solution became progressively yellow. The reaction mixture was stirred under reflux for 2 h and then it was evaporated to dryness under reduced pressure to give a pale yellow solid, which was dissolved in CH₂Cl₂ and precipitated with n-hexane yielding 63 mg (0.026 mmol) of microcrystalline powder of **2** (yield 72%). ¹H NMR (toluene-*d*₈, 300 K) δ 9.09 (dd, 1H, ³J_{HH} 5.8 Hz, ⁴J_{HH} 1.4 Hz, H5'), 8.25 (d, 1H, ³J_{HH} 1.9 Hz,

H10), 8.13 (d, 1H, ³J_{HH} 1.9 Hz, H11), 7.22 (d, 1H, ³J_{HH} 2.0 Hz, H6), 7.13 (hidden d, 1H, ³J_{HH} 2.0 Hz, H7), 7.11 (s, 1H, H2), 6.61 (ddd, 1H, ³J_{HH} 7.6 Hz, ³J_{HH} 6.6 Hz, ⁴J_{HH} 1.0 Hz, H4'), 6.53 (ddd, 1H, ³J_{HH} 7.8 Hz, ³J_{HH} 6.6 Hz, ⁴J_{HH} 1.4, H3'), 6.15 (dd, 1H, ³J_{HH} 7.8 Hz, ⁴J_{HH} 1.0 Hz, H2'). ¹³C NMR (DMSO-*d*₆, 300 K) δ 192.8 (CO), 192.5 (CO), 191.8 (CO), 191.7 (CO), 191.3 (CO), 191.1 (CO), 190.8 (CO), 190.7 (CO), 188.5 (CO), 156.6 (CH5'), 151.3 (C1'), 138.3 (CH3'), 137.9 (C8a), 135.1 (CH2), 137.8 (C4a), 134.5 (CH6), 133.5 (C12a), 133.4 (CH10), 130.2 (CH2'), 125.4 (CH4'), 116.5 (CH11) 113.4 (CH7). ¹⁵N NMR (DMSO-*d*₆, 300 K) δ -147.4 (N6'), -149.8 (N1), -202.4 (N8), -209.5 (N9), -218.1 (N5), -226.1 (N12), -230.8 (N4). IR (toluene) ν(CO): 2047 (m), 2044 (m, sh), 2040 (w), 2030.5 (s), 1945 (m, sh), 1938 (s), 1916 (vs), 1906 (m, sh) cm⁻¹. Elemental anal. calcd for C₄₆H₁₈Cl₆N₁₄O₁₈Re₆: C 23.15, H 0.75, N 8.22. Found: C 23.17, H 0.75, N 8.21. Pale yellow single crystals of **2** were obtained from slow diffusion of n-hexane into a CH₂Cl₂ saturated solution of **2**, at 248 K for a few days.

4.3. Crystal Structure Analysis

Singe-crystal X-ray diffraction data have been collected on a Bruker ApexII CCD diffractometer using graphite-monochromated Mo K α radiation ($\lambda = 0.71073 \text{ \AA}$). Low-temperature data collections have been performed employing a Cryostream 600 (Oxford Cryosystems). For all the species, a full sphere of reciprocal space has been collected, granting data completeness up to at least $(\sin \theta)/\lambda = 0.625 \text{ \AA}^{-1}$. CCDC 2214632–2214633 contain the supplementary crystallographic data for the paper. These data can be obtained free of charge from the Cambridge Crystallographic Data Centre.

Crystal Data for 1. C₁₇H₉ClN₇O₃Re, *M_r* = 580.96 u, monoclinic, space group *P*2₁/*c* (No. 14), *a* = 11.6604(11), *b* = 9.5472(9), *c* = 17.1011(16) Å, $\beta = 108.955(1)^\circ$, *V* = 1800.5(3) Å³, *Z* = 4, *d*_{calc} = 2.143 g cm⁻³, *T* = 150(2) K, crystal size = 0.490 × 0.120 × 0.050 mm³, $\mu = 6.934 \text{ mm}^{-1}$. Refinement of 262 parameters on 5686 independent reflections out of 40304 measured reflections (*R*_{int} = 0.0197, *R* _{σ} = 0.0120, 2 θ _{max} = 63.1°) led to *R*₁ = 0.0114 [*I* > 2 σ (*I*)], *wR*₂ = 0.0276 (all data), and *S* = 1.077, with the largest peak and hole of 0.499 and -0.658 e Å⁻³. To all the non-hydrogen atoms were given anisotropic displacement parameters. All the hydrogen atoms were clearly seen in a difference Fourier map; they were added in idealized positions and refined riding on their parent atom with an isotropic displacement parameter 1.2 times that of the pertinent parent atom.

Crystal Data for 2·4(n-hexane). C₄₆H₁₈Cl₆N₁₄O₁₈Re₆·4(C₆H₁₄) = C₇₀H₇₄Cl₆N₁₄O₁₈Re₆, *M_r* = 2729.33 u, monoclinic, space group *Cc* (No. 9), *a* = 14.0102(15), *b* = 35.458(4), *c* = 18.735(2) Å, $\beta = 110.310(2)^\circ$, *V* = 8728.5(16) Å³, *Z* = 4, *d*_{calc} = 2.077 g cm⁻³, *T* = 150(2) K, crystal size = 0.370 × 0.040 × 0.030 mm³, $\mu = 8.541 \text{ mm}^{-1}$. Refinement of 1028 parameters (applying 146 restraints) on 17863 independent reflections out of 77173 measured reflections (*R*_{int} = 0.0473, *R* _{σ} = 0.0458, 2 θ _{max} = 52.7°) led to *R*₁ = 0.0365 [*I* > 2 σ (*I*)], *wR*₂ = 0.0786 (all data), and *S* = 1.073, with the largest peak and hole of 0.816 and -0.838 e Å⁻³. Flack absolute structure parameter *x* = 0.009(8), based on 6980 (*I*⁺ - *I*⁻)/(*I*⁺ + *I*⁻) quotients (Friedel coverage: 99.7%). To all

the non-hydrogen atoms were given anisotropic displacement parameters. All the hydrogen atoms were added in idealized positions and refined riding on their parent atom with an isotropic displacement parameter 1.2 (or 1.5) times that of the pertinent parent atom. The four *n*-hexane solvate molecules were refined applying soft restraints on bond distances and bond angles, based on the mean values obtained from a survey of the Cambridge Structural Database (version 5.43, March 2022).³¹

4.4. Electrochemical characterization

The electrochemical investigation on complexes **1** and **2** was carried out by cyclic voltammetry at 0.2 V/s (and also at different scan rates in the case of stable complex **1**), in CH₃CN at 2.5×10⁻⁴ M concentration with 0.1 M tetrabutylammonium hexafluorophosphate TBAPF₆ (Aldrich) as supporting electrolyte, in a glass minicell (working volume 3 cm³), at 298 K. The working electrode was a GC disk (AMEL, diameter 3 mm), a Pt wire as counter electrode and an aqueous saturated calomel electrode SCE as operating reference electrode, inserted in a glass compartment ending with a porous frit and filled with the working medium, to prevent KCl and water leakage from the reference electrode into the working solution. Nitrogen was bubbled through a presaturator filled with the working solvent and then into the working cell in order to remove oxygen from the solution; during measurements it was kept above the working solution. The reversible CV pattern of the intersolvental reference redox couple ferricinium|ferrocene was recorded in the same operating conditions, determining its E°Fc⁺|Fc formal potential as the forward and backward peak average, to which the potentials were afterwards referred, thus eliminating the intersolvental junction potential. The measurements were carried out by an Autolab potentiostat managed by a PC with GPES software. The ohmic drop was corrected by the positive feedback method.

4.5. Photophysical characterization.

Photophysical measurements were carried out in air-equilibrated toluene solutions at room temperature or in the solid state. Electronic absorption spectra of solutions were recorded on an Agilent Model 8543 spectrophotometer at room

temperature, using quartz cells with a 1.0 cm path length. Steady-state emission spectra were recorded on an Edinburgh FLS980 spectrometer equipped with a 450 W ozone-free xenon arc lamp, double grating excitation and emission monochromators (2 × 300 mm focal length) and a Hamamatsu R928P photomultiplier tube. Time-resolved measurements were performed using the time-correlated single-photon counting (TCSPC) option on the FLS980, using as excitation source a microsecond flash Xe-lamp (60W, 0.1÷100 Hz). The emission was collected by a multichannel plate MCP-PMT Hamamatsu H10720-01 single-photon-counting detector. The photons collected at the detector were correlated using a time-to-amplitude converter (TAC) to the excitation pulse. The data analysis was performed using the commercially available F980 software (Edinburgh Instruments). The goodness of the data fitting was assessed by minimizing the reduced chi-squared function (χ^2). Photoluminescence quantum yields (Φ) were collected on an optically diluted solution (< 10⁻⁵ M) using wavelength scanning with a Hamamatsu C11347-11 Quantaaurus-QY Absolute PL quantum yield spectrometer, equipped with a xenon light source (150 W), a monochromator, and a Spectralon integrating sphere, and employing the commercially available U6039-05 PLQY measurement software (Hamamatsu Photonics Ltd, Shizuoka, Japan). The photoluminescence quantum yields were measured by exciting the samples between 340 and 400 nm.

Conflicts of interest

There are no conflicts to declare.

Acknowledgements

This work is supported by Università Degli Studi di Milano (projects PSR2021_DIP_005_PI_CDPIN and PSR2021_DIP_005_PI_DCARL). The use of instrumentation purchased through the Regione Lombardia-Fondazione Cariplo joint SmartMatLab Project is gratefully acknowledged.

References and Notes

1 For OLED devices see for instance: (a) H.-T. Mao, G.-F. Li, G.-G. Shan, X.-L. Wang, Z.-M. Su, *Coord. Chem. Rev.*, 2020, **413**, 213283; (b) X. Wu, M. Zhu, D. W. Bruce, W. Zhu, T. Fleetham, G. Li, J. Li *Adv. Mater.*, 2017, **29**, 1601861; for imaging and sensing see for instance: (c) C.-C. L. Lee, K. -W. K. Lo, *J. Am. Chem. Soc.*, 2022, **144**, 14420; (d) C.-C. L. Lee, K. -W. K. Lo, *Chem. Asian J.*, 2022, **17**, e202200840; for solar energy conversion see for instance: (e) A. Hagfeldt, G. Boschloo, L. Sun, L. Kloo, H. Pettersson, *Chem. Rev.*, 2010, **110**, 6595–6663; for photocatalysis see for instance: (f) C. K. Prier, D. A. Rankic, D. W. C. MacMillan, *Chem. Rev.*, 2013, **113**, 5322–5363.

2 (a) E. Cariati, A. Forni, E. Lucenti, D. Marinotto, A. Previtali, S. Righetto, C. Botta, V. Bold, V. C. Kravtsov, M.S. Fonari, *Chem. Asian J.*, 2019, **14**, 853–858; (b) M. S. Fonari, V. C. Kravtsov, V. Bold, E. Lucenti, E. Cariati, D. Marinotto, A. Forni, *Cryst. Growth Des.*, 2021, **21**, 4184–4200; (c) E. Lucenti, E. Cariati, A. Previtali, D. Marinotto, A. Forni, V. Bold, V. C. Kravtsov, M. S. Fonari, S. Galli, L. Carlucci, *Cryst. Growth Des.*, 2019, **19**, 1567–1575; (d) D. Malpicci, E. Lucenti, A. Forni, D. Marinotto, A. Previtali, L. Carlucci, P. Mercandelli, C. Botta, S. Righetto, E. Cariati, *Inorg. Chem. Front.*, 2021, **8**, 1312–1323; (e) E. Melnic, V. C. Kravtsov, E. Lucenti, E. Cariati, A. Forni, N. Siminel, M. S. Fonari, *New J. Chem.*, 2021, **45**, 9040–9052.

3 E. Lucenti, A. Forni, A. Previtali, D. Marinotto, D. Malpicci, S. Righetto, C. Giannini, T. Virgili, P. Kabacinski, L. Ganzer, *Chem. Sci.*,

2020, **11**, 7599–7608.

4 D. Malpicci, D. Blasi, D. Marinotto, A. Forni, E. Cariati, E. Lucenti, L. Carlucci, *Crystals*, 2023, **13**, 149.

5 (a) A. Vogler, H. Kunkely, *Coord. Chem. Rev.*, 2000, **200–202**, 991–1008; (b) A. Kumar, S.-S. Sun, A. J. Lees, *Top. Organomet. Chem.*, 2010, **29**, 1–35; (c) A. Vlček, *Top. Organomet. Chem.*, 2010, **29**, 73–114.

6 M. Wrighton, D. L. Morse, *J. Am. Chem. Soc.*, 1974, **96**, 998–1003.

7 (a) C.-C. Ko, A.-W.-Y. Cheung, L.-T.-L. Lo, J.-W.-K. Siu, C.-O. Ng, S.-M. Yiu, *Coord. Chem. Rev.*, 2012, **256** 1546–1555; (b) H. Takeda, K. Koike, T. Morimoto, H. Inumaru, O. Ishitani, R.V. Eldik, G. Stochel, *Adv. Inorg. Chem.*, 2011, 137–186; (c) C. Daniel, *Coord. Chem. Rev.*, 2015, **282–283** 19–32; (d) A. Vlcek, S. Zalis, *Coord. Chem. Rev.*, 2007, **251**, 258–287; (e) R.A. Kirgan, B.P. Sullivan, D.P. Rillema, *Top. Curr. Chem.*, 2007, **281** (Photochemistry and Photophysics of Coordination Compounds II) 45–100; (f) M. Panigati, M. Mauro, D. Donghi, P. Mercandelli, P. Mussini, L. De Cola, G. D'Alfonso, *Coord. Chem. Rev.*, 2012, **256**, 1621–1643.

8 (a) K. K.-W. Lo, K. Y. Zhang and S. P.-Y. Li, *Eur. J. Inorg. Chem.*, 2011, **2011**, 3551–3568; (b) K. K.-W. Lo, *Acc. Chem. Res.*, 2015, **48**, 2985–2995; (c) V. Fernandez-Moreira, F.L. Thorp-Greenwood, M.P. Coogan, *Chem. Commun.*, 2010, **46** 186; (d) K.K.-W. Lo, *Top. Organomet. Chem.* 2010, **29** 115; (e) E.A. Hillard, G. Jaouen, *Organometallics*, 2011, **30** 20; (f) S. Cauteruccio, E. Licandro, M. Panigati, G. D'Alfonso, S. Maiorana, *Coord. Chem. Rev.*, 2019, **386**, 119–137.

9 (a) G.-W. Zhao, J.-H. Zhao, Y.-X. Hu, D.-Y. Zhang, X. Li, *Synth. Met.*, 2016, **212**, 131–141; (b) For OLED devices see for instance: X. Li, D. Zhang, H. Chi, G. Xiao, Y. Dong, S. Wu, Z. Su, Z. Zhang, P. Lei, Z. Hu, W. Li, *Appl. Phys. Chem.*, 2010, **97**, 263303; (c) For polymer light emitting devices see for instance: L. Qian, D. Bera, P.H. Holloway, *Appl. Phys. Lett.*, 2007, **90**, 103511; (d) M. Mauro, C.-H. Yang, C.-Y. Shin, M. Panigati, C.-H. Chang, G. D'Alfonso, L. De Cola, *Adv. Mater.* 2012, **24**, 2054–2058.

10 (a) M. Schulz, M. Karnahl, M. Schwalbe and J. G. Vos, *Coord. Chem. Rev.*, 2012, **256**, 1682–1705; (b) A. Zarkadoulas, E. Koutsouri, C. Kefalidi and C. A. Mitsopoulou, *Coord. Chem. Rev.*, 2015, **304–305**, 55–72.

11 (a) C. Sun, S. Prosperini, P. Quagliotto, G. Viscardi, S. S. Yoon, R. Gobetto, C. Nervi, *Dalton Trans.*, 2016, **45**, 14678–14688; (b) S. Sung, D. Kumar, M. Gil-sepulcre, M. Nippe, *J. Am. Chem. Soc.*, 2017, **139**, 13993–13996; (c) D. A. Popov, J. M. Luna, N. M. Orchanian, Ralf Haiges, C. A. D. C., S. C. Marinescu, *Dalton Trans.* 2018, **47**, 17450–17460; (d) R. Kamata, H. Kumagai, Y. Yamazaki, G. Sahara, O. Ishitani, *ACS Appl. Mater. Interfaces*, 2019, **11**, 5632–5641; (e) S. Yang, W. Hu, X. Zhang, P. He, B. Pattengale, C. Liu, M. Cendejas, I. Hermans, X. Zhang, J. Zhang, et al., *J. Am. Chem. Soc.*, 2018, **140**, 14614–14618; (f) E. Quartapelle Procopio, A. Boni, L. Veronese, M. Marcaccio, P. Mercandelli, G. Valenti, M. Panigati, F. Paolucci, *ChemElectroChem* 2021, **8**, 2065–2069.

12 (a) A. S. Polo, M. K. Itokazu and N. Y. Murakami Iha, *Coord. Chem. Rev.*, 2004, **248**, 1343–1361.; (b) L. Veronese, E. Quartapelle Procopio, T. Moehl, M. Panigati, K. Nonomura A. Hagfeldt, *Phys.Chem.Chem.Phys.*, 2019, **21**, 7534.

13 L. C.-C. Lee, K.-K. Leung, K. K.-W. Lo, *Dalton Trans.*, 2017, **46**,16357.

14 (a) R. Q. Snurr, J. T. Hupp, S. T. Nguyen, *Acc. Chem. Res.* 2004, **37**, 1090–1095; (b) S. T. Nguyen, D. L. Gin, J. T. Hupp, X. Zhang, *Proc. Natl. Acad. Sci. U. S. A.* 2001, **98**, 11849–11850; (c) P. H. Dinolfo, J. T. Hupp, *Chem. Mater.* 2001, **13**, 3113–3125

15 D. Gupta, M. Sathiyendiran, *ChemistrySelect*, 2018, **3**, 7439–7458

16 R. Carballo, E. Garcia-Martinez, G. Pereiras-Gabian, E. M. Vazquez-Lopez, *Z. Naturforsch.* 2003, **58b**, 1021;

17 E. W. Abel, G. B. Hargreaves, G. Wilkinson, *J. Chem. Soc.*, 1958, 3149.

18 Two polymorphs and a pseudopolymorph of the free ligand have been characterized, see ref 3.

19 E. Melnic, V.Ch. Kravtsov, E. Lucenti, E. Cariati, A. Forni, N. Siminel and M.S. Fonari, *New J. Chem.*, 2021, **45**, 9040–9052.

20 A.C.C. Wong, G. Wilkinson, B. Hussain, M. Motevalli, M.B. Hursthouse, *Polyhedron* 1988, **7**, 1363–1370

21 J. Mukiza, T.I.A. Gerber, E.C. Hosten, R. Betz, *Z. Kristallogr. - New Cryst. Struct.*, 2014, **229**, 355–356.

22 M. Magni ,E. Lucenti, A. Previtali, P. R. Mussini, E. Cariati, *Electrochimica Acta*, 2019, **317**, 272-280.

23 It is worthwhile noting that the electrochemical characterization of free ligand was performed in dimethyl-formamide, unlike the present study in acetonitrile; however, in both cases potentials were normalized vs the formal potential of the intersolvental reference standard Fc⁺/Fc measured in the same conditions, which eliminates offsets related to differences in the intersolvental junction potentials; moreover, the effects of solvents DMF and CH₃CN in electrode processes are usually similar.

24 Complex **1** is stable in the working CH₃CN + 0.1 M TBAPF₆ medium and its electrode processes result in negligible surface conditioning, a favourable feature enabling to record many subsequent CV patterns with no need of frequent electrode polishing.

25 It is worthwhile underlining that, although CV patterns have been normalized by concentration besides electrode surface and square root of potential scan rate, we would refrain from a quantitative comparison of complex **2**, complex **1** and ligand peak current densities for a deeper insight in the electrode process mechanisms. In fact, besides some concentration uncertainty due to the very small weighed quantities and/or to stability/solubility issues, diffusion coefficients should remarkably decrease from ligand to complex **1** and complex **2**, resulting in significantly lower current densities at equal concentration; and in the case of complex **2** also issues concerning simultaneous availability of all redox active sites should be taken into consideration.

26 J. V. Caspar, T. J. Meyer, *J. Phys. Chem.*, 1983, **87**, 952–957.

27 (a) Y. Hong, J. W. Y. Lam, B. Z. Tang, *Chem. Soc. Rev.*, 2011, **40** 5361–5388; (b) J. Mei, Y. Hong, J. W. Y. Lam, A. Qin, Y. Tang, B. Z. Tang, *Adv. Mater.* 2014, **26**, 5429–5479.

28 (a) A. Poirot, C. Vanucci-Bacqué, B. Delavaux-Nicot, N. Leygue, N. Saffon-Merceron, F. Alary, F. Bedos-Belval, E. Benoist, S. Fery-Forgues, *Dalton Trans.*, 2021, **50**, 13686; (b) J. Wang, A. Poirot, B. Delavaux-Nicot, M. Wolff, S. Mallet-Ladeira, J. P. Calupitan, C. Allain, E. Benoista, S. Fery-Forgues, *Dalton Trans.*, 2019, **48**, 15906.

Journal Name

ARTICLE

29 B. Manimaran, P. Thanasekaran, T. Rajendran, R.-J. Lin, I.-J. Chang, G.-H. Lee, S.-M. Peng, S. Rajagopal, K.-L. Lu, *Inorg. Chem.*, 2002, **41**, 5323–5325.

30 (a) P. Thanasekaran, C.-C. Lee, K.-L. LU, *Acc. Chem. Res.* 2012, **45**, 1403-1418; (b) R. Nagarajapakash, R. Govindarajan, Bala. Manimaran, *Dalton Trans.*, 2015, **44**, 11732.

31 C.R. Groom, I.J. Bruno, M.P. Lightfoot and S.C. Ward, *Acta Crystallogr., Sect. B: Struct. Sci., Cryst. Eng. Mater.* 2016, **72**, 171–179.

View Article Online
DOI: 10.1039/D3NJ02823B

